

Research on Engineering Structures & Materials



www.jresm.org



Design and construction of full octagonal transducerbased low-cost dynamometer for measuring cutting forces during turning process

Agus Susanto, Budi Setiyana, Rifky Ismail, Risma Alfiyani

Online Publication Date: 30 December 2024

URL: http://www.jresm.org/archive/resm2024.448st0814rs.html

DOI: http://dx.doi.org/10.17515/resm2024.448st0814rs

Journal Abbreviation: Res. Eng. Struct. Mater.

To cite this article

Susanto A, Setiyana B, Ismail R, Alfiyani R. Design and construction of full octagonal transducer-based low-cost dynamometer for measuring cutting forces during turning process. *Res. Eng. Struct. Mater.*, 2025; 11(5): 2119-2137.

Disclaimer

All the opinions and statements expressed in the papers are on the responsibility of author(s) and are not to be regarded as those of the journal of Research on Engineering Structures and Materials (RESM) organization or related parties. The publishers make no warranty, explicit or implied, or make any representation with respect to the contents of any article will be complete or accurate or up to date. The accuracy of any instructions, equations, or other information should be independently verified. The publisher and related parties shall not be liable for any loss, actions, claims, proceedings, demand or costs or damages whatsoever or howsoever caused arising directly or indirectly in connection with use of the information given in the journal or related means.



Published articles are freely available to users under the terms of Creative Commons Attribution - NonCommercial 4.0 International Public License, as currently displayed at here (the "CC BY - NC").



Research on Engineering Structures & Materials



www.jresm.org

Research Article

Design and construction of full octagonal transducer-based low-cost dynamometer for measuring cutting forces during turning process

Agus Susanto 1,*,a, Budi Setiyana 2,b, Rifky Ismail 2,c, Risma Alfiyani 1,d

¹Lab. of Precision Engineering, Faculty of Engineering, State Polytechnic of Madiun, Indonesia ²Department of Mechanical Engineering, Faculty of Engineering, Diponegoro University, Indonesia

Article Info

Article History:

Received 14 Sep 2024 Accepted 22 Dec 2024

Keywords:

Full octagonal ringshaped transducer; Dynamometer; Cutting forces; Calibrations; Machining tests

Abstract

This research focuses on developing a low-cost dynamometer based on a novel transducer, full octagonal ring, which was used to a sensing element of cutting forces in turning process. Various evaluations were performed which aiming to produce accurate dynamometer. Static analysis showed that proposed transducer was capable of withstanding normal load of 224 N and tangential load of 388 N with stress, strain, and deflection of 233 MPa, 9.9×10 -4, and 8.5×10 -2 mm, respectively. The dynamic aspect indicated that the natural frequency of developed dynamometer could stabilize at 3.85 kHz with stiffness constant, k, damping ratio, ζ , and damping coefficient, c, of 18.5 × 10-6 N/m, 1.04%, 16 N-s/m. The calibration tests showed that the dynamometer sensitivity for normal force was 78.1 mV/N with cross sensitivity and linearity error values of 10.2% and 0.63%. The sensitivity for tangential force was 85.7 mV/N with cross sensitivity and linearity errors of 8.98% and 3.7%. The performance evaluation of dynamometer through machining tests proved that measured cutting forces matched well to the simulation ones. The spectrum frequencies also revealed characteristics of turning process. These results show that the developed dynamometer in this study was valid used for measuring cutting forces.

© 2025 MIM Research Group. All rights reserved.

1. Introduction

The machining process is a sequential and systematic stage to transform raw materials into products that have functions in a mechanical system. This process is a chain of manufacturing processes that are widely used in industry, wheatear drilling, milling, sawing, grinding, broaching, shaping, and turning processes. From the various types of machining processes, turning is a cutting process that is almost certainly applied to manufacture a product in many industries [1], wheatear it is for processing automotive components [2], aircraft [3], railways [4,5], HDPE-100 pipe [6], and others [7]. The interaction of the cutting-tool and the workpiece during turning process produces cutting forces that induce vibration, deformation, raising cutting temperature, and accelerate tool wear during machining process [8–10]. The cutting forces, therefore, has direct implications for the success of the machining process.

When it is possible to measure the cutting forces during the machining accurately and interpret them correctly, then the machining process can be optimized, tool wear might be monitored in real time, and even cutting errors can be minimized [11,12]. Cutting forces during turning process are generally measured using a piezoelectric-based commercial table dynamometer, which are installed on the machine's tool-post [13–15]. Zheng et al. [14] clamped Kistler 9257 table

*Corresponding author: agus_eng.dept@pnm.ac.id

^aorcid.org/0000-0001-9588-8484; ^borcid.org/0000-0003-1498-0735; ^corcid.org/0000-0003-0445-3405;

dorcid.org/0009-0002-8586-6083

DOI: http://dx.doi.org/10.17515/resm2024.448st0814rs

Res. Eng. Struct. Mat. Vol.11 Iss. 5 (2025) 2119-2137

dynamometer on the tool-post of CA6240 lathe machine for measuring forces during Titanium alloy machining. Fodor et al. [16] measured the cutting forces on dried orthogonal turning Aluminum alloy of AL2024-T351 using a Kistler 9129 dynamometer. A six-component table dynamometer was also used to acquire the cutting forces in hard turning of chrome molybdenum 42CrMo24-type alloy by [17]. However, the price of piezoelectric-based dynamometers, which reaches thousands of dollars, is not seen as cheap by some campus academics, researchers, and industrial operators to implement a machining process monitoring system through observation of cutting forces. Moreover, disassembling-assembling the lathe's tool-post first to install the table dynamometer is a bit of a tedious job. To overcome this problem, researchers have actually proposed low-costbased dynamometers. You et al. [18] developed cutting forces measurement tool based on strain gauges by applying the transducer model of two perpendicular octagonal rings (TPOR). Their developed dynamometer had sensitivity of 0.32 mV/N and natural frequency of 771 Hz, and it had been applied for measuring the cutting forces during AISI 1045 and Aluminum alloy turning process. However, they used commercial data acquisition that had not been included in production costs in the development of dynamometers. Uquillas et al. [19,20] developed a force measuring tool by utilizing strain gauges with wireless transmission technology.

Rizal et al. [21,22] focused on designing and manufacturing the dynamometers based on both octagonal ring and cross beam transducer models. They claimed that their developed dynamometer had a dynamic response of about 766 Hz, sensitivity of 3.13–172.4 mV/N, 0.87% in cross-sensitivity error, and appropriate for acquiring cutting forces about 3 kN. Korkut [23], Yaldiz et al. [24,25] developed instrument for measuring cutting forces based on the octagonal ring. They implemented it in either turning or milling processes. The eight-shaped rings transducer-based dynamometer was developed for measuring milling forces [26]. Various transducer models were applied as an essential element composing dynamometer, including circular ring [27], diaphragm type [28], elastic body [29], bending beam [30,31], hexagonal ring [32], square ring [33], octagonal-elliptical ring [34–38], and two extended octagonal rings [39].

Based on those studies, one of the important components of composing a dynamometer is the transducer. It was used as a sensing element for measuring cutting forces during machining. The design of the transducers that has an inner circular shape, such as octagonal ring transducers [22–25,34–38,40], circular rings [27], and the eight-shaped (ES) [26], has a shortcoming in the sensor installation. Those transducers caused the strain gauge installed on the inside of transducer to experience initial compression, even when the load had not been applied. This clearly effects on the accuracy of cutting forces measurements. Therefore, an alternative transducer design needs to be studied, that can be worked to sense cutting forces in turning process precisely.

This study focuses on designing, analyzing, and fabrication of low-cost dynamometer based on proposed novel transducer, namely full octagonal ring-shaped transducer. Various evaluations were performed which aiming to produce accurate and reliable dynamometer, which cover static and dynamic analysis, and calibration tests. Following, machining tests were conducted to evaluate the performance of the developed dynamometer for acquiring cutting forces during turning process. In the following sections, cutting forces model in turning operation is first explained in Section 2. The materials and methods are following discussing in Section 3. The results and discussions of the study are described in Section 4, which include static and dynamic analysis of transducer, configuration of the developed dynamometer and its calibrations, evaluating the performance of the developed dynamometer through various machining tests.

2. Cutting Forces Model During Turning Process

Turning process is applied to cylindrical workpiece for producing parts that are basically round in shape, either external or internal shapes [41]. In orthogonal turning process, a workpiece is cut using a cutting tool with the angle of cutting-edge perpendicular to the cutting direction as shown in Fig. 1. From Fig. 1(a), the rotating workpiece with the rotational speed of ω (rpm) is cut by a sharp cutting tool that moves translationally along the cutting length with axial cutting depth of a (mm) and feeding speed of V_f (mm/min.). During machining, the cutting forces are generated that

cause plastic deformation on the workpiece material and producing in chips. These cutting forces acting in turning process are shown in Fig. 1(b).

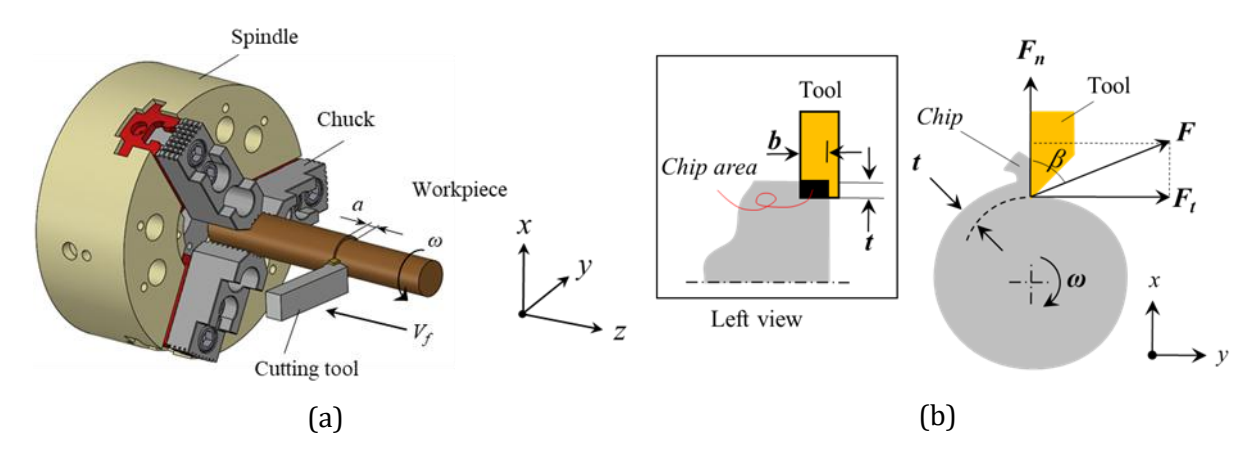


Fig. 1. Cutting process in turning (a) Turning process and its machining parameters and (b)

Cutting forces generated during turning process

Based on Fig. 1(b), the cutting force, F (N), acting during turning process is proportional to the specific cutting force, Ks (N/mm²), multiplied by cross-sectional area of chip, A_C (mm²), which is formulated as [42]s;

$$F = A_c \cdot K_s \tag{1}$$

The cutting force can then be decomposed into normal, F_n , and tangential, F_t , force components by cutting force angle, β . They are calculated as follows;

$$F_t = Ks.b.a.\sin\beta \tag{2}$$

$$F_n = Ks \cdot b \cdot a \cdot \cos \beta \tag{3}$$

where *b* is chip thickness.

3. Methods

3.1. Developed Transducer

The method used in this study was a development and construction model that aims to produce an accurate, precise, and reliable dynamometer when used for measuring cutting forces in turning process. The development of dynamometers focused on the transducer which is one of the urgent components of composing a dynamometer that functions as a sensing element of cutting forces. This study proposed a full octagonal shaped ring transducer model as displayed in Fig. 2(a) in developing dynamometer. The material of this component was steel with dimensions of width, thickness, and ring radius of 15 mm, 3 mm, and 13.5 mm, respectively. It is seen that the transducer is different from the octagonal-elliptical ring-shaped transducers used by [21,23-26,36], and others [35,38]. Those old transducer models caused the sensor attached to the transducer's inner surface having pre-compressive, even when the forces had not been applied as shown in Fig. 2(b). This obviously affected the accuracy and reliability of the cutting forces measurement. On the other hand, the proposed transducer in this study does not cause pre-compressive in sensor as shown in Fig. 2(c), so that the precision of the measurement of the cutting force – in the initial assumption – is more guaranteed. Various evaluations were performed which aiming to produce accurate dynamometer, namely; (1) static analysis, (2) dynamical test, transducer and dynamometer calibrations, and machining tests.

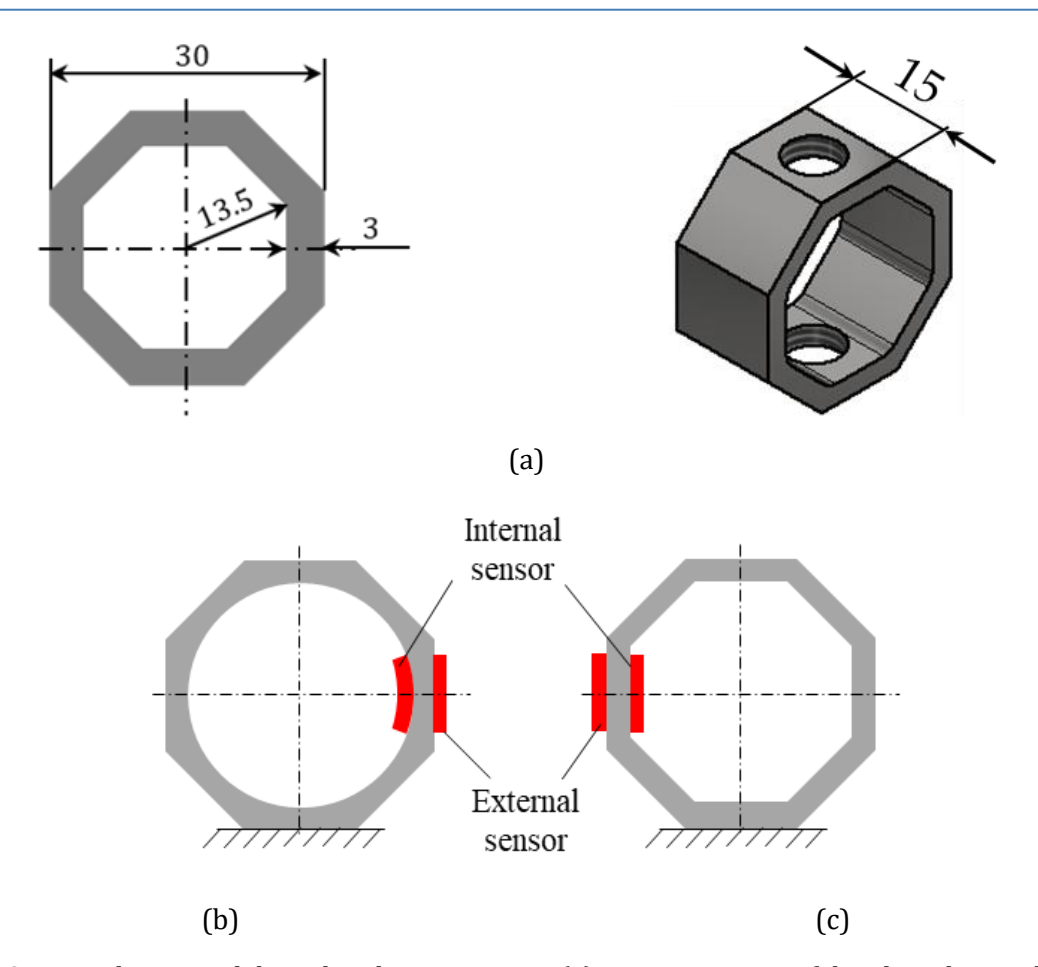


Fig. 2. Transducer model used in dynamometer: (a) isometric view of developed transducer and its dimension, (b) pre-compressive effect on the sensor using old transducer, (c) no pre-compressive effect on the sensor using proposed transducer model

3.2 Static Analysis Based on The Finite Element Method (FEM)

Static analysis based on the finite element method (FEM) is performed to evaluate the strength of the developed transducer structure against the applied loads. Fig. 3 displays the meshing in FEM environment. Type meshing of 3D Hexahedrons with 91015 nodes and 59671 elements was used in the calculation. Five types of meshing independence tests including skewness index, element quality parameters, orthogonal quality, aspect ratio, and parallel deviation were conducted to determine the meshing quality. The results showed that the meshing was verified to be able to proceed to the next analysis step.

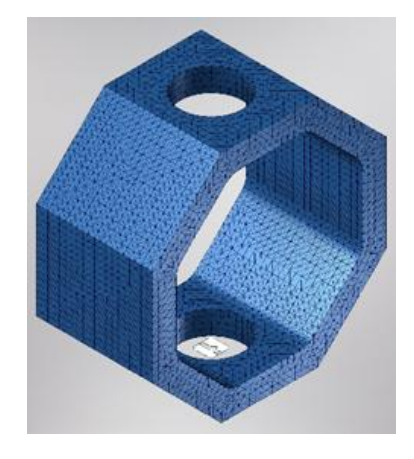


Fig. 3. Meshing of developed transducer in FEM environment

3.3. Test of Dynamical Characteristic of Transducer

During turning process, the cutting forces are not in a static situation, but also dynamic [8]. Therefore, it is also important to consider the system response to dynamic loads. And, the component of dynamometer that is most susceptible to dynamic problems is the transducer. In this case, the dynamic response of the dynamometer structure is influenced by the forced frequency of the spindle rotation. During machining process, the natural frequency and forced frequency must be very different from each other. This will ensure that the cutting force obtained will not be affected by dynamic phenomena caused by the construction of the dynamometer.

For identifying the dynamical behavior of transducer, the test – well-known as hammering tests – was carried out. Fig. 4 shows the experimental hammering test along with the instruments needed in the tests. It is seen that the transducer is excited by an Dytran 5800B3 electrical hammer, so that the structure vibrates. The transient external force of the excitation was measured by a piezotronics embedded in the hammer tip and the vibration response was quantified by an Dytran 3413A2 less-mass accelerometer attached to the structure. Those instruments had been activated by an Omega power supply. Both impulse forces and vibration responses were then acquired by a data storage oscilloscope, GW Instek, where the data can be checked by a software-interfaced personal computer. To ensure the data were based on correct assumptions, a certain amount of collecting data, 3-5 times the replication were collected which were then averaged.

Data Acquisition system kx $m\ddot{x}$ Transducer $c\dot{x}$ Impact hammer Accelerometer x(t)Response Impulse force

Fig. 4. Schematic diagram of hammering test

Based on the single degree of vibration model shown in Fig. 4, the vibration equation can be written by summing inertial, damping, stiffness and external forces as follows:

$$m\ddot{x} + c\dot{x} + kx = Fe^{i\omega t} \tag{4}$$

where m, c, and k are dynamic modal parameters of mass (kg), stiffness constant (N/m), and damping coefficient (N-s/m), respectively. $Fe^{i\omega t}$ is the transient impulse force in function of frequency (ω, Hz) , with $i=\sqrt{-1}$ is an imaginary value. While, $x=Xe^{i\omega t}$ is the deflection of transducer due to being hit by hammer and it can be derived into velocity and acceleration, which are $\dot{x}=i\omega Xe^{i\omega t}$ and $\ddot{x}=-\omega^2 Xe^{i\omega t}$. By substituting these deriving variables into Eq. (4) and eliminating the exponential numbers, the frequency response function (FRF) is obtained in the form of;

$$\frac{X}{F} = \frac{1}{-\omega^2 m + i\omega c + k} \tag{5}$$

Equation (5) can be decomposed into a pair of the real and imaginary parts of the FRF, namely:

$$\operatorname{Re}(G(f)) = \frac{(1-r^{2})}{k((1-r^{2})^{2} + (2\zeta r)^{2})}$$

$$\operatorname{Im}(G(f)) = \frac{-2\zeta f}{k((1-r^{2})^{2} + (2\zeta r)^{2})}$$
(6)

Where ζ is the damping ratio and the ratio between frequency function to the natural frequency is shown by $r = \frac{\omega}{\omega_n}$. Furthermore, the equations of the real and imaginary parts of the FRF formulated in Eq. (6) can be depicted in Fig. 5.

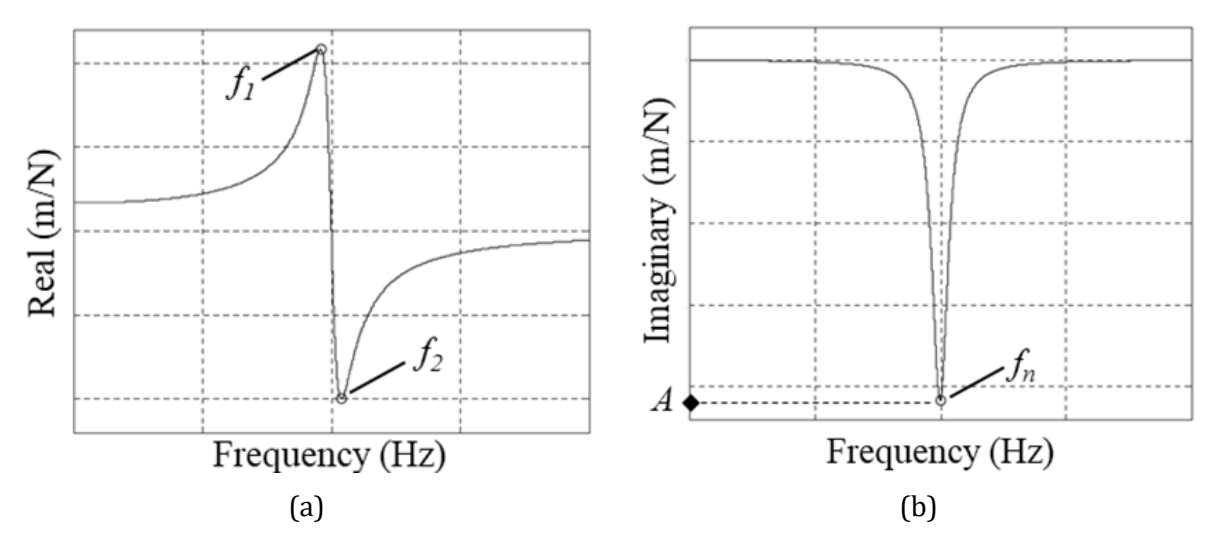


Fig. 5. A pair of FRF parts that are "measured" from testing (a) Real part and (b) Imaginary part

It can be seen that each peak is identified with small circles in both figures, namely f_n , f_1 , and f_2 (Hz) and A (m/N). They are indispensable for extracting dynamic modal parameters of transducer. Following are four steps to extract them;

- Find a damping ratio ζ (%) by $\zeta = \frac{f_2 f_1}{2f_n}$
- Find the constant stiffness k (N/m) through $k = -\frac{1}{2A\zeta}$.
- Convert the natural frequency fn (Hz) to ω_n (radian/s) by multiplying 2π to get compatible units and use $\omega_n = \sqrt{\frac{k}{m}}$ to calculate the modal mass m (kg).
- Finally, calculate $c = 2\zeta \sqrt{km}$ to determine the damping coefficient c (N-s/m).

3.4 Dynamometer Configures and Data Acquisition System

The configuration and orientation of the transducer on the developed dynamometer is shown in Fig. 5. It can be seen that the sensors of strain gauges that are attached to the transducer with a certain configuration and orientation to produce the shape of the dynamometer as shown in Fig. 6(a). The configuration and orientation of the transducer were intended for measuring normal (F_n) and tangential (F_t) cutting forces during the turning process as discussed in Section 2. For each measurement of the force component, the strain gauges are assembled based on Wheatstone bridges as seen in Fig. 6(b).

To measure the tangential force, transducers A and B in Fig. 6(a) are attached to a series of strain gauges whose arrangement is shown in Fig. 6(b-right). It can be seen that there are four strain gauges (R1, R2, R3 and R4) that are connected based on the Wheatstone bridge. R1 and R3 are

attached on the outer surface of the transducer at an angle of 45° to the vertical plane that would be subjected to tensile stress. R2 and R4 are attached on the outer surface of the transducer at an angle of 45° to the vertical plane so that they would be subjected to compressive stress. For measuring normal force (F_n), transducers A, B, C and D in Fig. 6(b) are attached with eight strain gauges which the arrangements are shown in Fig. 5(b-left). R5, R7, R9 and R11 are attached on the outer surface of the transducers at an angle of 90° to the vertical plane that would be subjected to tensile stress. R6, R8, R10 and R12 are attached on the inner surface of the transducer with the perpendicular angle to the vertical plane that would be subjected to compressive stress. The strain gauges used were BF(BA)350-3AA with dimensions of 7.44×4.4 mm and a gauge factor was 2.0-2.2.

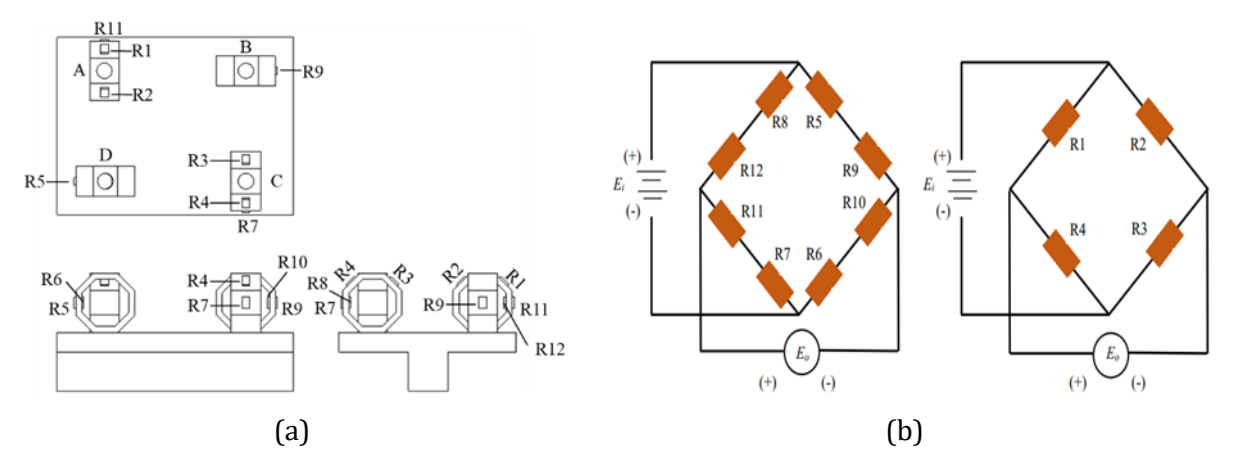


Fig. 6. Configuration and orientation transducer on developed dynamometer (a) Arrangement strain gauges that attached on transducer and (b) Wheatstone bridges-based order strain gauges for measure: (left) normal force, and (right) tangential force

3.5 Calibration Tests

To determine the characteristics of transducers and dynamometers due to the applied loads, calibration tests were conducted. The experimental set-up and schematic diagram for both the individual transducer and dynamometer are shown in Fig. 7. Fig. 7(a) shows the experimental set-up and the instruments required in the calibration. It can be seen that the instruments needed for the calibration test include; units tested either dynamometer or transducer, calibration test-rig, wire sling, load, data acquisition system, and PC laptop.

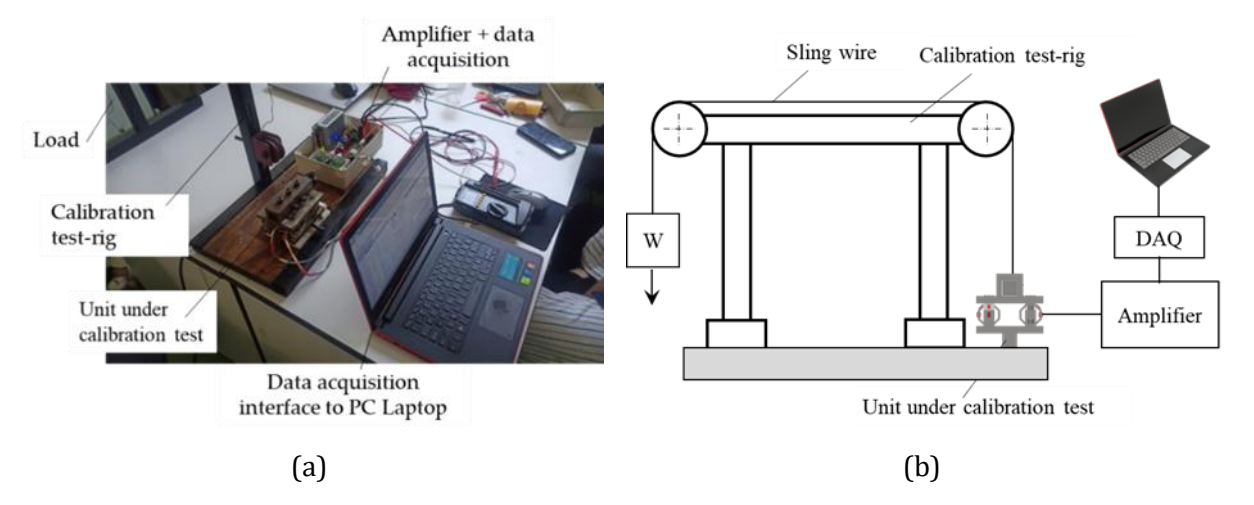


Fig. 7. Experimental set-up and schematic diagram for calibration tests (a) Instruments required for calibration tests and (b) Schematic diagrams of calibration tests; individual transducer or constructed dynamometer

Fig. 7(b) shows a schematic diagram of the calibration on the unit under test, either an individual transducer or constructed dynamometer. In the calibration of the individual transducer, the structure was subjected to a load that ranged from 0 to 60 N with a step addition of 10 N, where the load was connected by a sling wire. The loading was intended to evaluate the sensing of transducer to the given loads, both the outer part and the inner part of transducer (see Fig. 2). In addition, calibration due to cross-load effect was also observed to evaluate the transducer response due to cross-load, both the normal response due to the tangential load, and the tangential response due to the normal load. In the calibration of a constructed dynamometer, the tests were performed on two orientations of the force component; F_n and F_t , with gradual loading until reaching 100 N with a load interval of 10 N. To ensure the consistency of the output results, the tests were repeated 3 times. The results of the calibration test were then used to evaluate cross-sensitivity and linearity errors. In addition, a linear equation was also obtained based on this calibration.

3.6 Machining Tests

The next tests were conducted for evaluating the performance of the developed dynamometer in measuring the cutting forces. Dry machining was carried out on the ANNYANG conventional lathe machine. The experimental set-up of the cutting process is shown in Fig. 8. Based on Fig. 8(a), a 1045 carbon steel workpiece with 25 mm in diameter and a length of 100 mm is clamped on the machine spindle. Tool holder of DASAN MWLNR (20×20 mm) with insert cutting tool of tungsten carbide (WNMG0804) is clamped on a developed dynamometer by M8 bolts and it was mounted on the tool-post of machine. The installation of the developed dynamometer was easy to use than measuring the cutting force using a piezoelectric-based table dynamometer as it had been commonly used [14,43]. This is because, the installation of dynamometer did not need to disassemble-assemble the tool-post of machine.

Cutting forces measurement are carried out based on the schematic diagram as shown in Fig. 8(b). The machining process is performed at a constant cutting depth (a) of 0.2 mm, and a constant feed rate (f_r) of 0.06 mm/rev., and varying spindle rotational speed, ω , namely 160, 320, and 450 rpm. These machining parameters were similar to those used by other researchers when testing the dynamometers they developed [14,22,40].

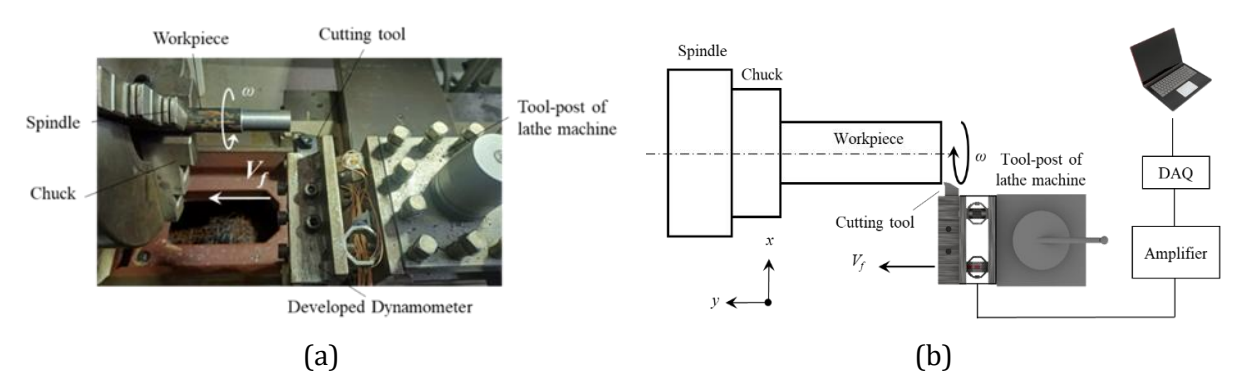


Fig. 8. Cutting tests conducted for developed performance evaluation (a) experimental set-up and (b) schematic diagram of the cutting test

4. Results and Discussions

4.1. Static And Dynamic Analysis of The Transducer

Static analysis based on the finite element method (FEM) is performed to evaluate the strength of the structure against the applied load. Fig. 9 displays the condition of the full octagonal shaped ring transducer which is subjected to normal force (F_n) and tangential force (F_t) of 224 N and 388 N evaluated based on FEM. Those conditions display distribution of stresses, strains, deflections, and safety factors.

Based on Fig. 9(a), the forces cause the transducer to having stress over the entire area with stress distribution ranging from 0.5 - 233 MPa as shown on the color bar. The part of the transducer that

is most having stresses when the forces were applied is indicated by red. Fig. 9(b) shows the strain distribution experienced by the transducer with a maximum strain of 9.9×10^{-4} . This maximum strain is relatively small which indicates that this transducer was quite rigid. The deflection is also fairly small, namely 8.541×10^{-2} mm as shown in Fig. 9(c). The transducer is rigidly designed to keep the turning forced frequency away from the natural frequency of developed dynamometer, so that the transducer was not going through damage due to the loads. Fig. 9(d) shows the safety factor analysis of the transducer which indicate that the transducer is still in a good condition to be used with the given loads. This is because the maximum stress that occurs had not reached the yield strength of the transducer material, 250 MPa.

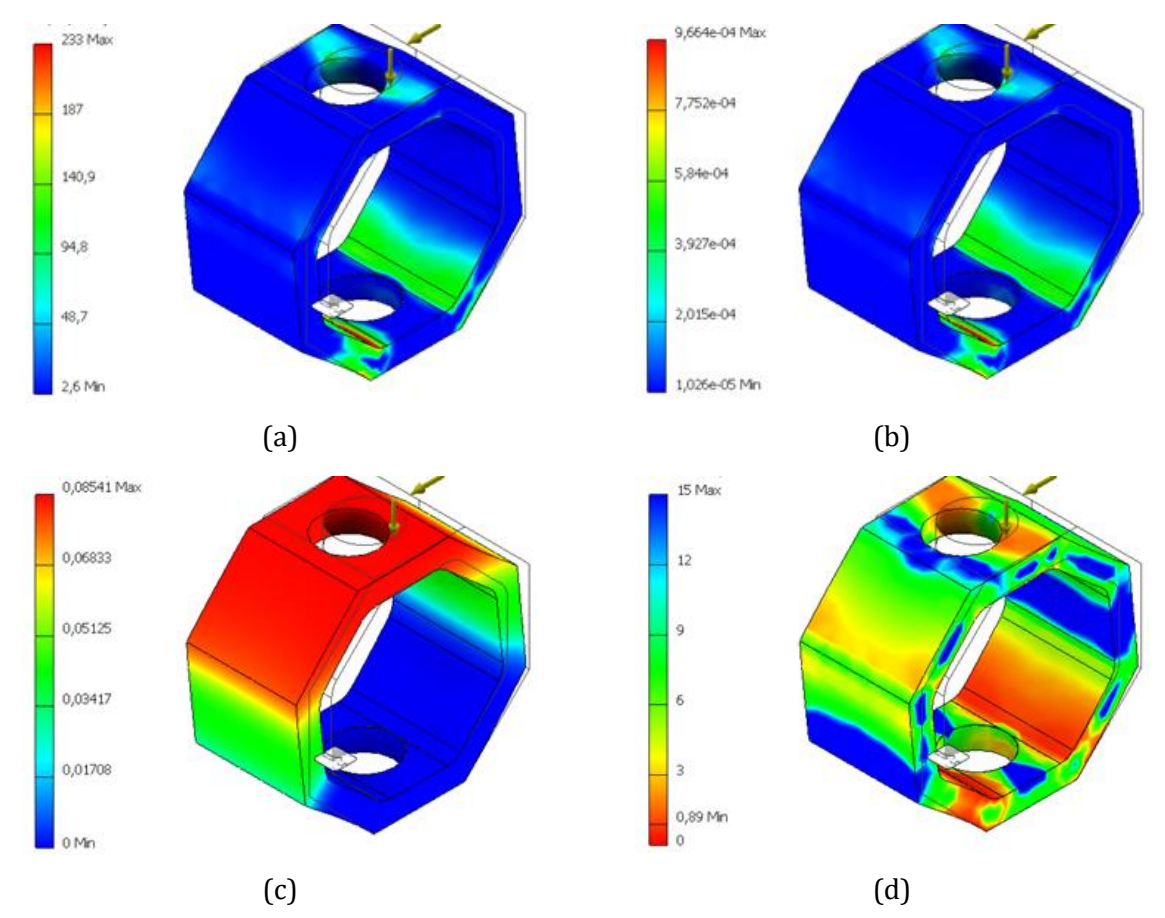


Fig. 9. Distribution of stresses, strains, displacements, and safety factors experienced the surface of the developed transducer when subjected by normal and tangential forces (a) Stress distribution (MPa), (b) Strain distribution, (c) Displacement distribution (mm) and (d) Safety factor distribution

The dynamic analysis based on the FEM are shown in Fig. 10, which shows the first four vibration modes experienced by the transducer due to the normal force and tangential force applied to the transducer. Fig. 10(a) shows the first vibration mode with a natural frequency of $3.85 \, \text{kHz}$. It can be seen that the transducer is deformed, but still maintain its shape. Figs. 10(b) - 9(d) show the second to fourth vibration modes with frequencies of 6.41, 14.1 and $20 \, \text{kHz}$, respectively. At these frequencies, the transducer undergoes a deformation due to dynamic loads and does not hold its initial shape. So, it is quite risky to use the developed dynamometer at those frequencies.

Fig. 11 displays raw data in the time domain data obtained by impact tests. They are the impulse force and vibration response which are shown in Figs. 11(a) and 11(b), respectively. It is seen that when the transducer was excited with a force of 1 N by hammer, the damped free vibration was given by structure. The oscillation decays over time and the vibration finally vanished. Those time domain data were then transformed into a frequency response function (FRF) to determine dynamic modal parameters of transducer in receiving dynamic loads. Fig. 12 is an FRFs consisting of the real and the imaginary parts of FRF. By utilizing these two graphs, the dynamic modal

parameters of transducer can be extracted based on the explanation in Section 3.2, as well as have been applied to mechanical structures in general, whether in precision table grinding [44], lathes [45], milling [46], drilling [47], and automotive vehicles [48]. The results of the extraction of dynamic modal parameters, which including mass (m), damping coefficient (c), stiffness (k), damping ratio (ζ) , and natural frequency (f_n) are tabulated in Table 1. These results are valid with simulation results based on FEM in previous discussion.

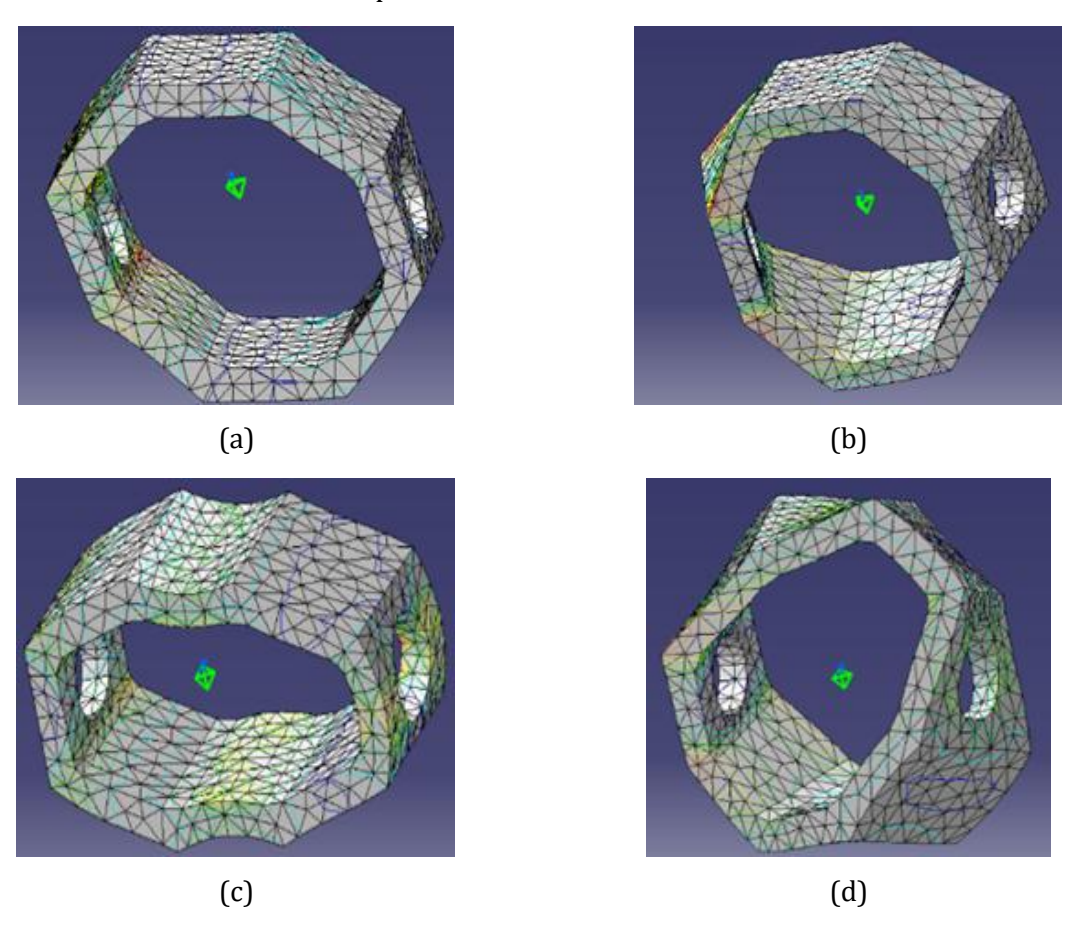


Fig. 10. The first four vibration modes of the transducer under the of applied forces (a) 1st mode, (b) 2nd mode, (c) 3rd mode and (d) 4th mode

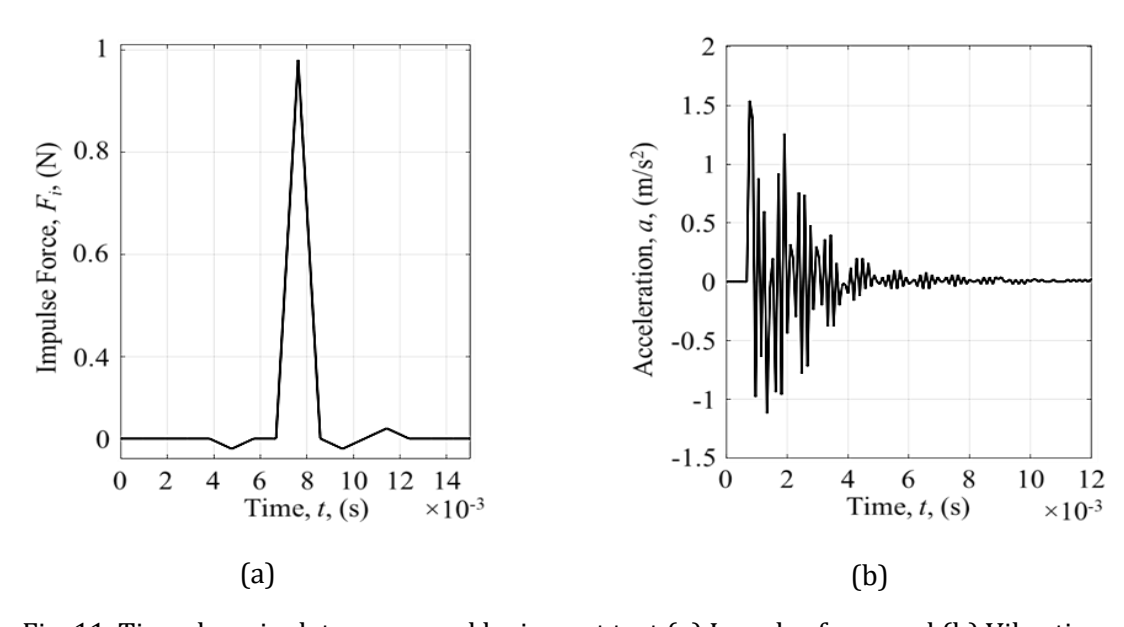
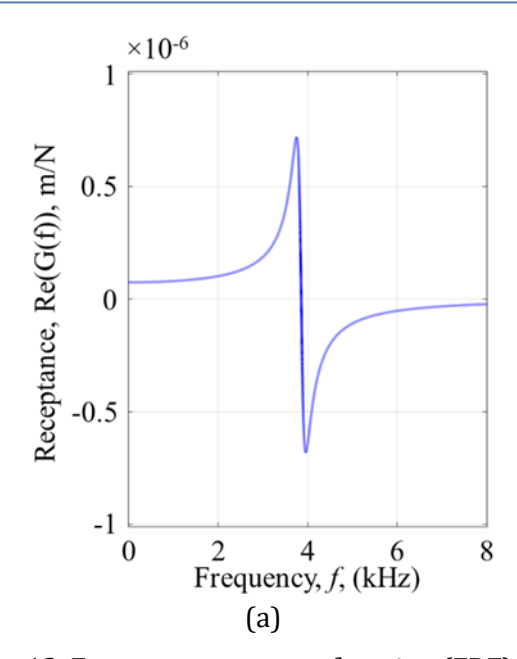


Fig. 11. Time domain data measured by impact test (a) Impulse force and (b) Vibration response



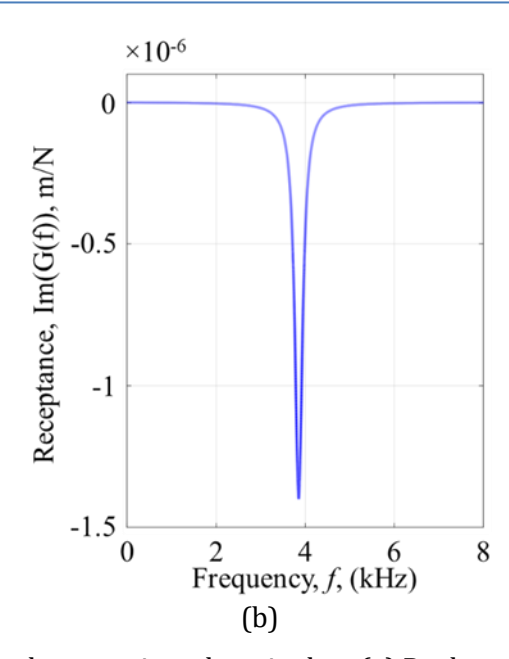


Fig. 12. Frequency response function (FRF) associated to raw time-domain data (a) Real part of FRF and (b) Imaginary part of FRF

Table 1. Parameter modal dynamic of transducer

Dynamic Parameters	Value
Mass (m)	32 g
Damping coefficient (c)	16 N-s/m
Stiffness (k)	18,5 x 10 ⁻⁶ N/m
Frequency (f_n)	3,85 kHz
Damping ratio (ζ)	1,04%

4.2 Calibration of Transducer

Calibration on individual transducer aims to evaluate the transducer through the response given by the transducer due to the load applied to it. Fig. 13 shows the output results during calibration tests. Fig. 13(a) shows the transducer calibration for normal response and Fig. 13(b) shows the transducer calibration in tangential response. Both Figs 13(a) and 13(b) show three data due to the load applied to the transducer through the experiment described in Fig. 7. The black and red graphs are responses sensed by sensors attached to the outer transducer and inner transducer, respectively, (see Fig. 2). The blue graph is the calibration of the transducer due to the cross-load effect which used to evaluate the transducer response in normal direction due to the application of tangential directional loads.

It can be seen that the normal load calibration for the external sensor above shows an upward trend with respect to the given load, while the normal load calibration for the inner sensor shows a downward trend. This shows that the measurement of normal loading using a developed transducer worked well. In addition, the blue graph indicates that the transducer is not affected by the cross-load effect, both the normal directional response due to tangential loading and the tangential directional response due to normal loading. This shows that the developed transducer measures the cutting force independently and was not affected by the directional loading.

In calibration test of the normal direction transducer, the regression equation was $y_n = 0.1425 \, \mathrm{x} - 0.0514$. Meanwhile, the root mean square error (RMSE) [49] for the data was 3.2%, and the mean absolute error (MAE) [13,16,49,50] was 2.4%. On the other hand, the regression equation of the transducer calibration resulted for the tangential direction of data was $y_t = 0.1379 \, \mathrm{x} - 0.0197$. The RMSE for the data was 2.5%. Meanwhile, the MAE for these three data was 2.1%. Those lower the RMSE and MAE indicated that calibration tests show the better the model performs.

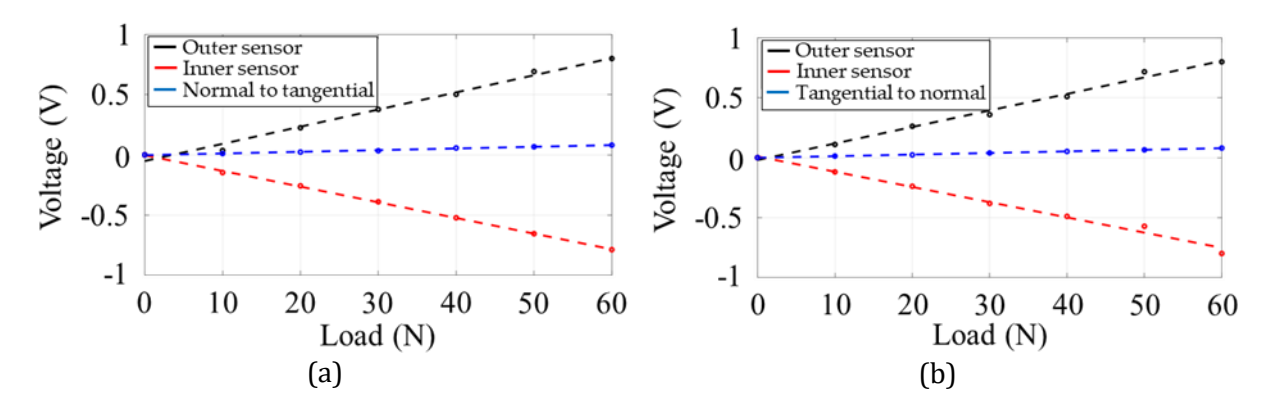


Fig. 13. The transducer calibration (a) normal, (b) tangential responses

4.3 Design and Construction of Low-Cost Dynamometer Based on Full Octagonal Transducer

Fig. 14 displays a construction of low-cost dynamometer based on a full octagonal shaped ring and the important other instrument to measure cutting forces in turning process. The configuration of the strain gauge installation on the transducer of dynamometer along with the necessary fittings is presented in Fig. 14(a). Besides, Fig. 14(b) is a prototype of developed dynamometer. The overall cost of producing these dynamometers is about 70% cheaper than the commercial piezoelectric dynamometers widely used by previous researchers [13,16,50].

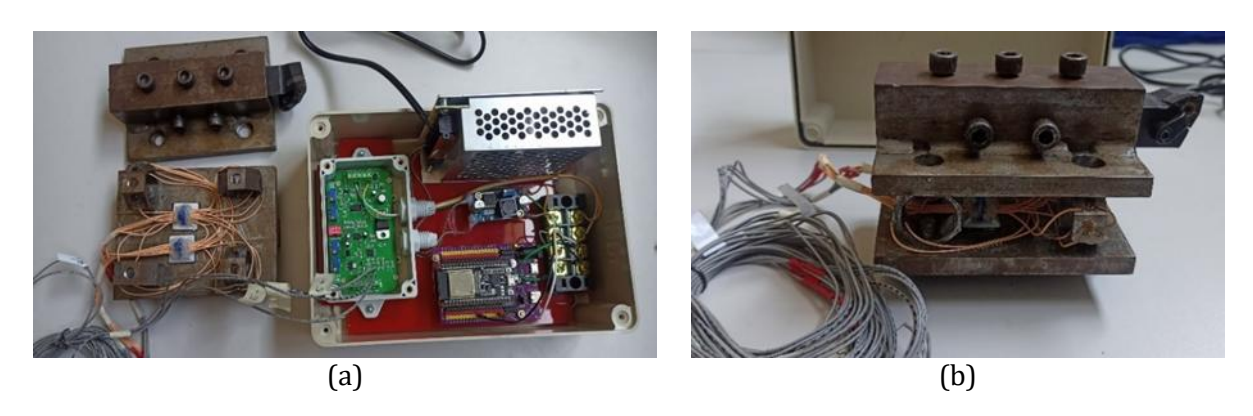


Fig. 14. Construction low-cost dynamometer base on full octagonal shaped ring and the essential components (a) Installation strain gauge on transducer and the data acquisition and (b) Prototype of developed dynamometer

This developed dynamometer consisted of upper and lower plates with dimensions of $120 \times 90 \times 10$ mm. The bottom plate was used to a handle to which the tool-post was attached. The top plate was used as a place for the cutting tool. Four transducers attached strain gauges with a wiring system were placed between the bottom and the top plates, which are then fastened by M8 nuts. Besides, other instruments in the developed dynamometer include a 24V power supply, step down, amplifier and ESP 32 acquisition data. This part was usually ignored in the development of low-cost dynamometers as shown in previous results [18,21,22].

4.3 Dynamometer Calibration

The dynamometer calibration results are shown in Fig. 15 where Fig. 15(a) is the dynamometer calibration for normal force, and Fig. 15(b) is for tangential force due to the loading applied. It can be seen that there are two graphs in each figure. The black curve is a dynamometer response due to direct load, namely; (a) normal force calibration due to normal load, and (b) tangential force calibration due to tangential load. Meanwhile, the red graph is a dynamometer response due to the cross-load effect, namely; (a) normal force calibration due to tangential loads, and (b) tangential force calibration due to normal loads.

Both black curves, both normal and tangential force calibrations, indicate an uptrend. The calibration sensitivity of the dynamometer to normal force was 78.1 mV/N. The linear regression equation of the test was $y_n = 0.0781 \text{x} + 0.014$, which RSME was 2.9%, and the MAE was 2.1%. Meanwhile, the calibration sensitivity of the dynamometer to the tangential force was 85.7 mV/N with a linear regression from data of $y_t = 0.0784 \text{x} - 0.0209$, which RMSE of 3.2% and MAE of 2.7%.

The cross effect of tangential load on the normal force for dynamometer calibration shows slight upward trend with a maximum error of 10.2%, so that the cross effect of tangential tool does not interfere with the normal force measurement on the dynamometer. From three tests, a regression equation was obtained, namely $y_{nct}=0.0014x-0.0018$, and they had RMSE of 0.17%, and MAE of 0.14%. Meanwhile, the cross effect of normal load on tangential force calibration was also insignificant and did not interfere to the measurement results with a maximum error of 8.98%. The regression of the test was $y_{tcn}=0.0029x-0.0097$. RMSE was 0.47%, and MAE was 0.37%.

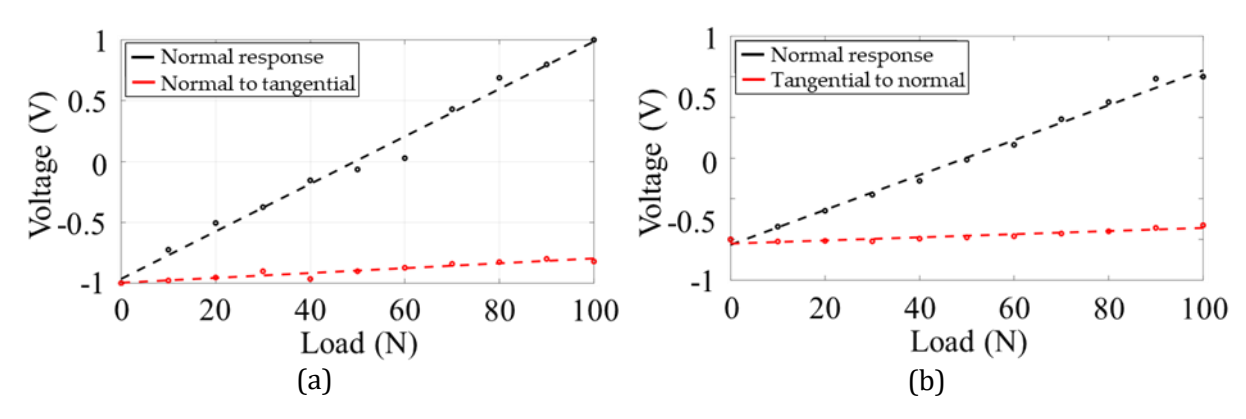


Fig. 15. Dynamometer calibrations (a) normal response, (b) tangential response due to the load application

The calibration was then used to evaluate linearity errors when a maximum load of about 100 N was applied to the dynamometer. It was found that the linearity error in normal force was 0.63% and for linearity error in tangential force was 3.7%. This means that the developed dynamometer was acceptable for measuring cutting forces in turning process.

4.4 Machining Tests

Machining tests are carried out to evaluate the cutting force measurement in turning process using a developed dynamometer. Fig. 16 shows cutting forces measured using developed dynamometer based on the variation in spindle rotational speed. Figs. 16(a), 16(b) and 16(c) show the cutting forces associated with spindle rotational speed of 160 rpm, 320 rpm, and 450 rpm, respectively. In addition of normal and tangential forces, resultant forces are also seen that were calculated by $F = \sqrt{F_t^2 + F_n^2}$. It is seen that the quantity of the cutting forces is similar. This indicated that variations in spindle rotation speed did not affect the quantity of cutting force, but they affected the cutting time; the greater the spindle rotation speed, the faster the machining process, and vice versa. This is because the quantity of the cutting force was affected by the axial depth of cut [42,51]. For all cutting experiments, it was seen that the normal force had a smaller quantity than the other cutting force.

From the figures, it is seen that the cutting forces fluctuate. These fluctuations were strongly influenced by the dynamic cutting process during contacted between the cutting-tool and the workpiece, noise from surrounding environment, namely from material factors and machine conditions [8,9]. Some theories such as Hamilton's principle need to be considered to ensure this phenomenon and considering the importance of static and dynamic analysis in structural design [52]. On the other hand, those cutting force trends had a good agreement with previous studies which used commercial dynamometers such as in [16,17,30]. In order to confirm above deduction and to evaluate the measurement results, cutting forces measured by the cutting tests were compared with calculated cutting forces, which the equations have been described in Section 2. The

comparison between the measured cutting forces to the simulation one is shown in Figs. 17, 18, and 19. Random noise has been added to the simulation, while considering other conditions are in the same as the conditions of machining tests. The specific cutting force, *Ks*, of 2600 N/mm² for 1045 carbon steel was applied in the simulation [53]. Based on the figures, the cutting forces obtained through experimental tests comparing to the simulation results show well agreement.

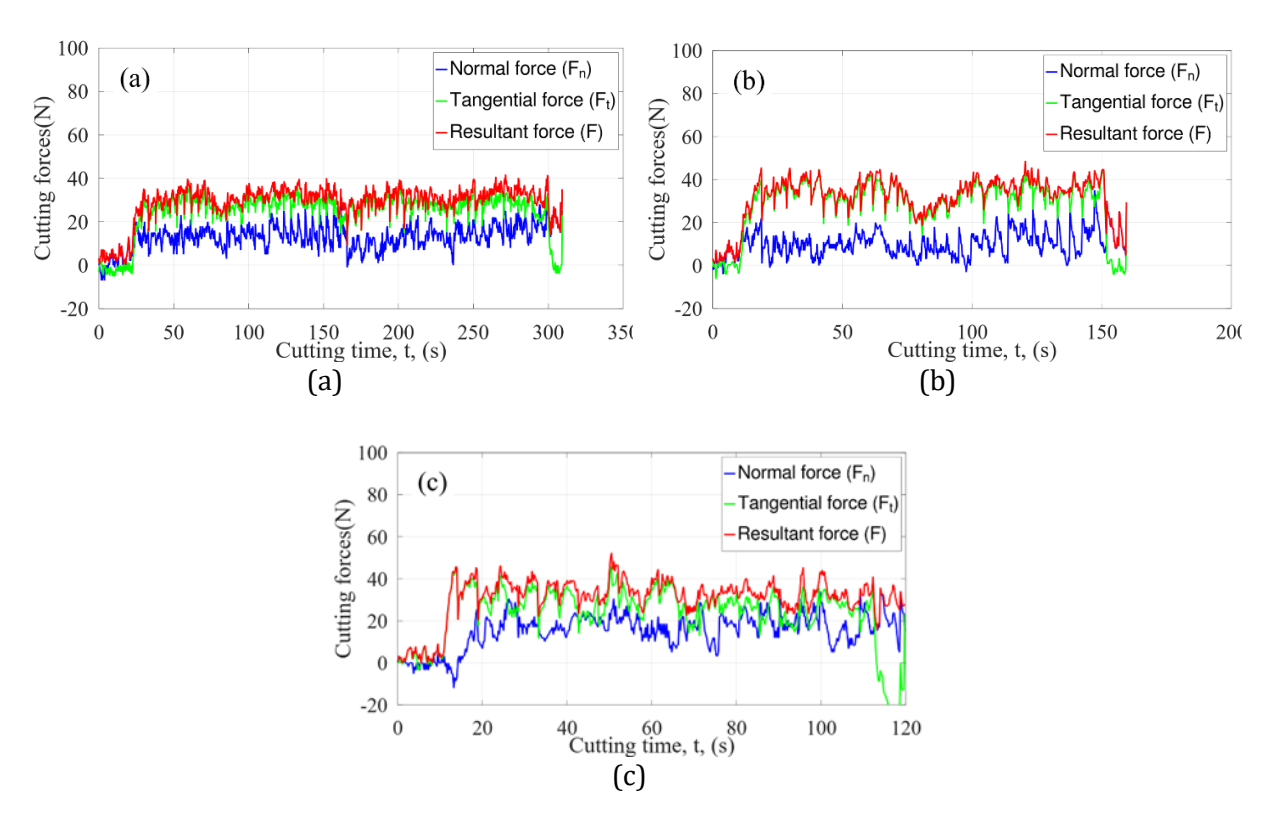


Fig. 16. Cutting forces measured by machining tests using developed dynamometer with the spindle rotation speed; (a) 160 rpm, (b) 320 rpm, and (c) 450 rpm

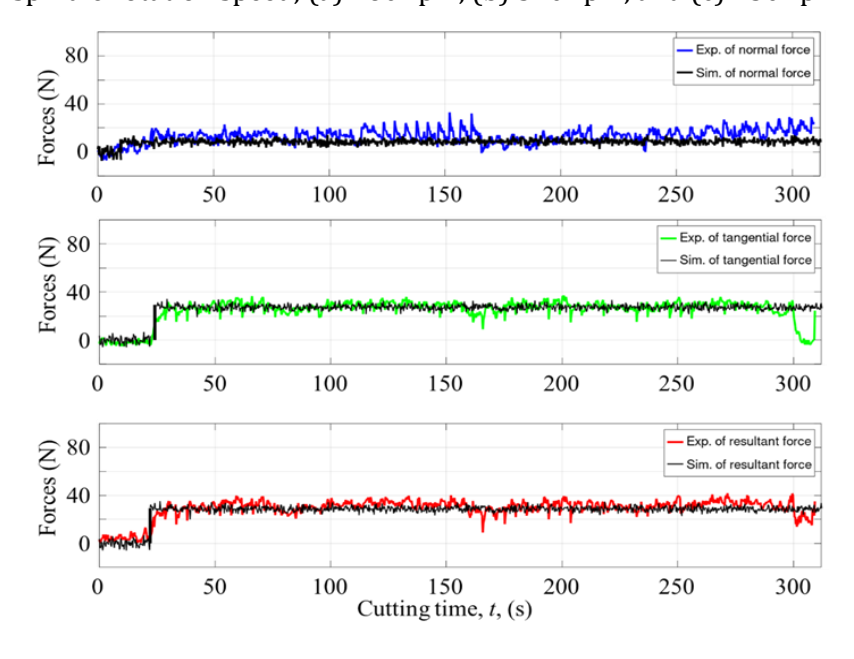


Fig. 17. Comparison of cutting force obtained by machining tests to the simulations for spindle rotation speed of 160 rpm

Fig. 17 shows cutting forces comparison between the measured to the simulation for spindle rotational speed of 160 rpm. Figs. 17(a), 17(b) and 17(c) represent the normal, tangential, and resultant cutting forces, respectively. It can be seen that the cutting time required to machine about

50 mm in cutting length is 313 seconds. The cutting force in the first 15 seconds is still close to zero, which indicates there was no cutting process occurred. When the cutting process has started until the end of the operation, the cutting forces are steady with certain quantity.

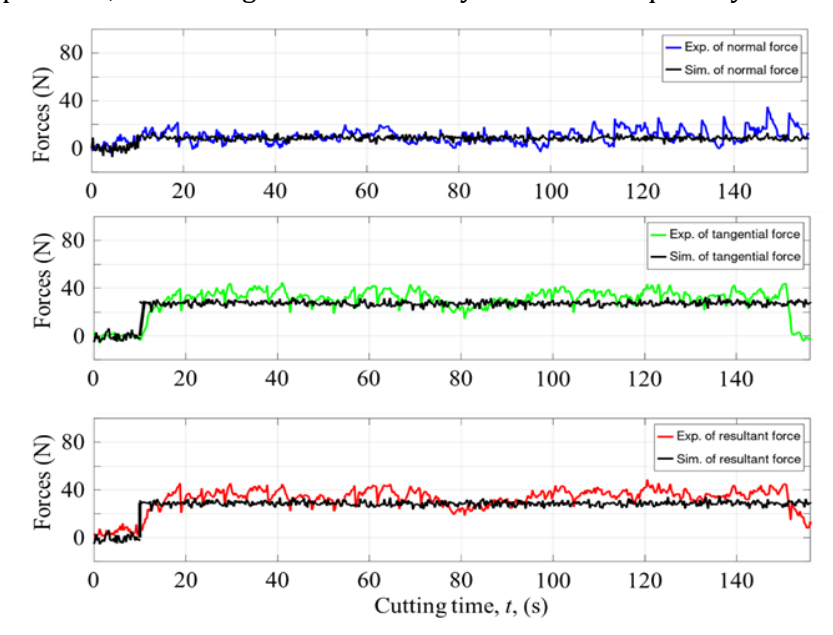


Fig. 18. Comparison of cutting force obtained by machining tests to the simulations for spindle rotation speed of 320 rpm

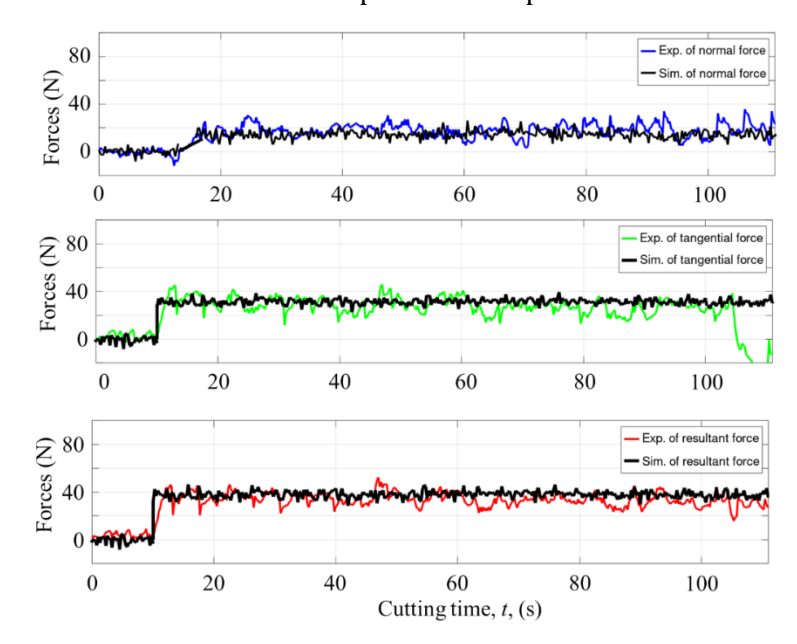


Fig. 19. Comparison of cutting force obtained by machining tests to the simulations for spindle rotation speed of 450 rpm

Fig. 18 displays cutting forces comparison for experiment with simulation one in spindle rotational speed of 320 rpm. With the same cutting length, the cutting time is twice as fast, which is 156 seconds. Fig. 19 is a comparison of the measured cutting forces to the simulation in a spindle rotational speed of 450 rpm. It is seen that the cutting time is faster than the other two, which is 111 seconds. To find out the effect of spindle speeds on the attributes of turning process, it was necessary to transform the cutting forces obtained in machining tests displayed in Fig. 16 to the frequency spectrum to observe the frequency characteristics of cutting. This is because the spindle rotational speed almost certainly affects the frequency content of the cutting process in machining process. The frequency spectrum calculated by fast Fourier transform (FTT) are shown in Fig. 20.

Those Figs. 20(a), 20(b) and 20(c) are frequency spectrum that correspond to cutting force of (a) 160 rpm, (b) 320 rpm, and (c) 450 rpm, respectively.

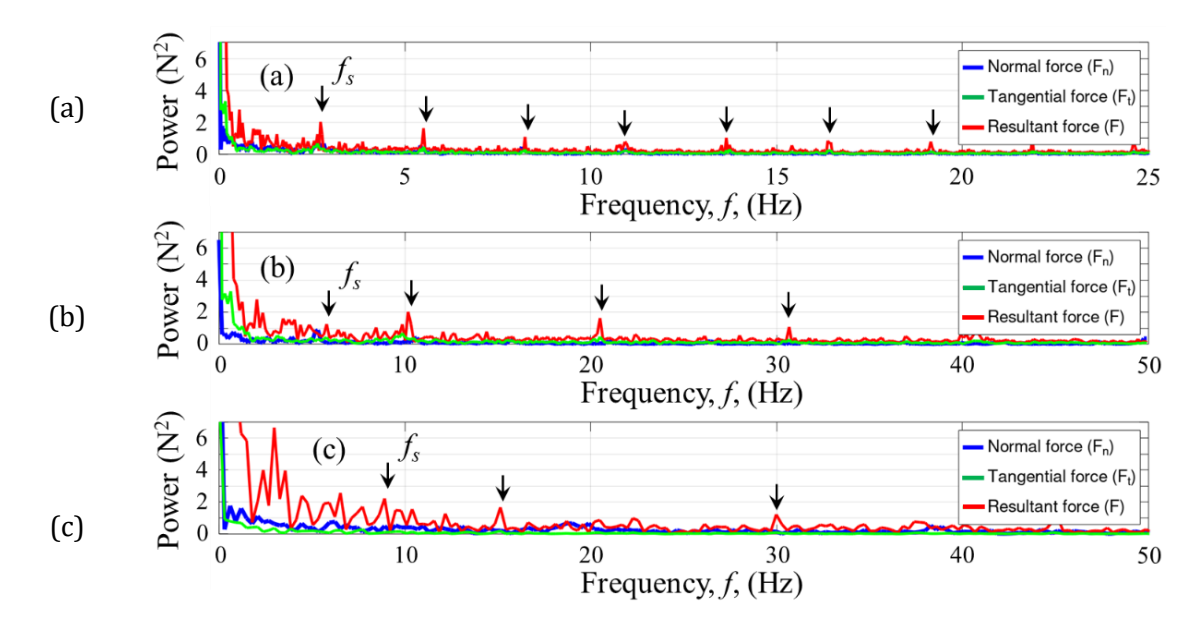


Fig. 20. The frequency spectrum of cutting forces measured during machining tests corresponding to; (a) 160 rpm, (b) 320 rpm, and (c) 450 rpm

The spectrum above shows the frequency content of the cutting forces, the normal, tangential, and resultant of cutting forces which are visualized with the colour of each graph. Based on each frequency spectrum above, there are various frequencies that are observed. They are spindle rotation frequency, f_s , and its harmonic frequencies marked by the arrow. Both the spindle and harmonic frequencies were characteristic frequencies which were a consequence of the machining process. Harmonic frequency was calculated by multiplication of f_s by integer numbers.

Based on the frequency spectrum in Fig. 20(a), the spindle frequency is 2.7 Hz. It was associated to spindle rotation speed of 160 rpm. This frequency is followed by its harmonic frequencies, namely 5.4, 8.1, 10.8, Hz and so on. From Fig. 20(b), it is found spindle rotational frequency of 5.4 Hz, which associated to spindle rotational speed of 320 rpm, and followed by its harmonic frequencies, namely 10.6 and 21.2 Hz. Frequency spectrum in Fig. 20(c) displays spindle rotational frequency of 7.5 Hz, which associated to spindle rotational speed of 450 rpm, and its harmonic frequencies at 15 and 30 Hz. All of these characteristic frequencies were typically forced vibration. These spectrum frequency results indicated that the developed dynamometer perform well. It was because the dynamometer revealed the characteristic frequencies during turning process.

5. Conclusions

This study discusses the low-cost dynamometer developed for measuring cutting forces during turning process. Owing to the transducer is one of the main components that is used to as a sensing element of cutting forces, a novel full-octagonal ring- shaped transducer was proposed to overcome the weaknesses of the inner circular ring-based transducer which has been introduced previously. Various evaluations were performed which aiming to produce accurate and reliable dynamometer, which cover static analysis by Finite Element Method (FEM), dynamic analysis by impact tests, and calibration tests. Finally, machining tests were conducted for varying the performance of the developed dynamometer. Based on the results and discussions, several important points are drawn as follows;

• Static analysis showed that the proposed transducer was capable of withstanding normal load of 224 N and tangential load of 388 N with stress, strain, and deflection of 233 MPa, 9.9 \times 10⁻⁴, and 8.5 \times 10⁻² mm, respectively. The transducer was also safe to use as indicated by the distribution of safety factors.

- The dynamic aspect indicated that the natural frequency of developed dynamometer could stabilize at 3.85 kHz with stiffness constant, k, damping ratio, ζ , and damping coefficient, c, of 18.5×10^{-6} N/m, 1.04%, 16 N-s/m, respectively.
- The calibration tests revealed that the sensitivity, cross sensitivity, and linearity errors for normal force were 78.1 mV/N, 10.2%, and 0.63%. Meanwhile, for tangential force was 85.7 mV/N in sensitivity with cross sensitivity and linearity errors were 8.98% and 3.7%, respectively.
- The cutting forces obtained during machining tests showed good agreement with the simulation-based cutting forces. It means that developed dynamometer was accurate for measuring cutting forces during turning process.
- The characteristic frequencies of cutting processes which were explored by fast Fourier transform showed that the developed dynamometer was valid used for measuring cutting forces in turning process. The frequency of rotational spindle and its harmonics appeared in the spectrum frequency.

Acknowledgment

Authors sincerely thank you to Diponegoro University which has funded this research during Postdoctoral Grant in World Class University Program.

References

- [1] Gasagara A, Jin W, Uwimbabazi A. Stability analysis for a single-point cutting tool deflection in turning operation. Advances in Mechanical Engineering. 2019;11(6):1-14. https://doi.org/10.1177/1687814019853188
- [2] Wang SM, Chen YS, Lee CY, Yeh CC, Wang CC. Methods of in-process on-machine auto-inspection of dimensional error and auto-compensation of tool wear for precision turning. Applied Sciences. 2016;6(5). https://doi.org/10.3390/app6040107
- [3] Shi D, Gindy NN. Development of an online machining process monitoring system: Application in hard turning. Sensors and Actuators A: Physical. 2007;135(2):405-14. https://doi.org/10.1016/j.sna.2006.08.011
- [4] Coromant S. Railway turning: Re-turning and new wheel turning. Sandvik Coromant. 2022.
- [5] Industry KR. Technical Information Korloy: Railway Industry. Korloy. 2022;
- [6] Mammeri S, Chaoui K, Bouacha K. Manufacturing of testing specimens from tough HDPE-100 pipe: Turning parameters optimization. Research on Engineering Structures & Materials. 2024;10(2):513-36.
- [7] Lukács J, Horváth R. Comprehensive Investigations of Cutting with Round Insert: Introduction of a Predictive Force Model with Verification. Metals. 2022;12(2). https://doi.org/10.3390/met12020257
- [8] Susanto A, Liu CH, Yamada K, Hwang YR, Tanaka R, Sekiya K. Application of Hilbert-Huang transform for vibration signal analysis in end-milling. Precision Engineering. 2018;53:263-77. https://doi.org/10.1016/j.precisioneng.2018.04.008
- [9] Susanto A, Liu C-H, Yamada K, Hwang Y-R, Tanaka R, Sekiya K. Milling Process Monitoring Based on Vibration Analysis Using Hilbert-Huang Transform. Int. J. of Automation and Technology. 2018;12(5):688-98. https://doi.org/10.20965/ijat.2018.p0688
- [10] Susanto A, Yamada K, Tanaka R, Handoko YA, Subhan MF. Chatter identification in turning process based on vibration analysis using Hilbert- Huang transform. Journal of Mechanical Engineering and Science. 2020;14(2):6856-68. https://doi.org/10.15282/jmes.14.2.2020.25.0537
- [11] Kim JH, Chang HK, Han DC, Jang DY, Oh SI. Cutting force estimation by measuring spindle displacement in milling process. CIRP Ann Manuf Technol. 2005;54(1):67-70. https://doi.org/10.1016/S0007-8506(07)60051-1
- [12] Lauro CH, Brandão LC, Baldo D, Reis RA, Davim JP. Monitoring and processing signal applied in machining processes A review. Measurement. 2014;58:73-86. https://doi.org/10.1016/j.measurement.2014.08.035
- [13] Stein JL, Huh K. Monitoring cutting forces in turning: A model-based approach. Journal of Manufacturing Science and Engineering. 2002;124(1):26-31. https://doi.org/10.1115/1.1432666
- [14] Zheng Q, Yang C, Zhang S, Hu Y. Simulation and experimental research on cutting force of turning titanium alloy. MATEC Web Conf. 2015;31:4-8. https://doi.org/10.1051/matecconf/20153103013
- [15] Krajcoviech S, Holubjak J, Richtarik M, Czánová T. Identification of process Prime A turning when machining steel C56E2 and monitoring of cutting forces. Transp Res Procedia. 2021;55:605-12. https://doi.org/10.1016/j.trpro.2021.07.027

- [16] Fodor G, Sykora HT, Bachrathy D. Stochastic modeling of the cutting force in turning processes. Int J Adv Manuf Technol. 2020;111(1-2):213-26. https://doi.org/10.1007/s00170-020-05877-8
- [17] Cahuc O, Gerard A, Bisu C, Ispas C. A force torsor analysis for a turning process in the presence of selfexcited vibrations. Appl Mech Mater. 2011;62:135-46. https://doi.org/10.4028/www.scientific.net/AMM.62.135
- [18] You Z, Yulong Z, Taobo G. Application of a strain gauge cutting force sensor in machining process monitoring. 2019 14th IEEE Int Conf Electron Meas Instruments, ICEMI 2019. 2019;891-7. https://doi.org/10.1109/ICEMI46757.2019.9101849
- [19] Reyes-Uquillas DA, Yeh SS. Tool holder sensor design for measuring the cutting force in CNC turning machines. IEEE/ASME Int Conf Adv Intell Mechatronics, AIM. 2015;2015-Augus:1218-23. https://doi.org/10.1109/AIM.2015.7222705
- [20] Reyes-Uquillas DA, Hsiao T. Wireless tool holder sensor design for cutting force measurement applied to chatter detection. IEEE Reg 10 Annu Int Conf Proceedings/TENCON. 2017;1845-8. https://doi.org/10.1109/TENCON.2016.7848340
- [21] Rizal M, Ghani JA, Husni, Husaini. Design and construction of a strain gauge-based dynamometer for a 3-axis cutting force measurement in turning process. J Mech Eng Sci. 2018;12(4):4072-87. https://doi.org/10.15282/jmes.12.4.2018.07.0353
- [22] Rizal M, Ghani JA, Mubarak AZ. Design and Development of a Tri-Axial Turning Dynamometer Utilizing Cross-Beam Type Force Transducer for Fine-Turning Cutting Force Measurement. Sensors. 2022;22(22). https://doi.org/10.3390/s22228751
- [23] Korkut I. A dynamometer design and its construction for milling operation. Mater Des. 2003;24(8):631-7. https://doi.org/10.1016/S0261-3069(03)00122-5
- [24] Yaldiz S, Ünsaçar F. Design, development and testing of a turning dynamometer for cutting force measurement. Mater Des. 2006;27(10):839-46. https://doi.org/10.1016/j.matdes.2005.04.001
- [25] Yaldiz S, Ünsaçar F, Sağlam H, Işik H. Design, development and testing of a four-component milling dynamometer for the measurement of cutting force and torque. Mech Syst Signal Process. 2007;21(3):1499-511. https://doi.org/10.1016/j.ymssp.2006.06.005
- [26] Mohanraj T, Deepesh T, Dhinesh R, Jayaprakash S, Sai Krishna S. Design and analysis of a strain gauge based eight-shaped elliptical ring dynamometer for milling force measurement. Proc Inst Mech Eng Part C J Mech Eng Sci. 2021;235(17):3125-34. https://doi.org/10.1177/0954406220967681
- [27] Kumar H, Sharma C, Kumar A, Arora PK, Kumar S. Design, development and metrological characterization of a low capacity precision industrial force transducer. ISA Trans. 2015;58:659-66. https://doi.org/10.1016/j.isatra.2015.07.011
- [28] Kumar R, Pant BD, Maji S. Development and Characterization of a Diaphragm-Shaped Force Transducer for Static Force Measurement. Mapan J Metrol Soc India. 2017;32(3):167-74. https://doi.org/10.1007/s12647-017-0207-7
- [29] Liu M, Zhang Z, Zhou Z, Peng S, Tan Y. A new method based on Fiber Bragg grating sensor for the milling force measurement. Mechatronics. 2015;31:22-9. https://doi.org/10.1016/j.mechatronics.2015.03.007
- [30] Şeker U, Kurt A, Çiftçi I. Design and construction of dynamometer for measurement of cutting forces during machining with linear motion. Mater Des. 2002;23(4):355-60. https://doi.org/10.1016/S0261-3069(02)00013-4
- [31] Xie Z, Lu Y, Li J. Development and testing of an integrated smart tool holder for four-component cutting force measurement. Mechanical System Signal Processing. 2017;93:225-40. https://doi.org/10.1016/j.ymssp.2017.01.038
- [32] Kumar H, Pardeep, Kaushik M, Kumar A. Development and Characterization of a Modified Ring Shaped Force Transducer. Mapan J Metrol Soc India. 2015;30(1):37-47. https://doi.org/10.1007/s12647-014-0118-9
- [33] Kumar H, Sharma C, Kumar A. The development and characterization of a square ring shaped force transducer. Meas Sci Technol. 2013;24(9). https://doi.org/10.1088/0957-0233/24/9/095007
- [34] Kroencke M, Hull ML. A method for designing multiload component dynamometers incorporating octagonal strain rings. Exp Mech. 1989;29(2):195-204. https://doi.org/10.1007/BF02321375
- [35] Dandage R V, Bhatwadekar SG, Bhagwat MM. Design , Development and Testing of a Four Component Milling Tool Dynamometer. Int J Appl Eng Technol. 2012;2(1):45-50.
- [36] Soliman E. Performance analysis of octal rings as mechanical force transducers. Alexandria Eng J [Internet]. 2015;54(2):155-62. https://doi.org/10.1016/j.aej.2015.01.004
- [37] Uddin MS, Songyi D. On the design and analysis of an octagonal-ellipse ring based cutting force measuring transducer. Meas J Int Meas Confed. 2016;90:168-77. https://doi.org/10.1016/j.measurement.2016.04.055
- [38] Pathri BP, Garg AK, Unune DR, Mali HS, Dhami SS, Nagar R. Design and Fabrication of a Strain Gauge Type 3-axis Milling Tool Dynamometer. Int J Mater Form Mach Process. 2016;3(2):1-15. https://doi.org/10.4018/IJMFMP.2016070101

- [39] Ammar AA, Jallouli M, Bouaziz Z. Design and development of a dynamometer for the simulation of the cutting forces in milling. Int J Autom Control. 2011;5(1):44-60. https://doi.org/10.1504/IJAAC.2011.037379
- [40] Rizal M, Ghani JA, Nuawi MZ, Haron CHC. Development and testing of an integrated rotating dynamometer on tool holder for milling process. Mech Syst Signal Process. 2015;52-53(1):559-76. https://doi.org/10.1016/j.ymssp.2014.07.017
- [41] Kalpakjian S, Schmid SR. Manufacturing Engineering and Technology. Prentice Hall International, Singapore. New Jersey: Prentice Hall Singapore; 2001.
- [42] Tony L. Schmitz, Smith KS. Machining Dynamics: Frequency Response to Improved Productivity. Vol. 1, Springer. 2008. 1-303 p.
- [43] Amigo FJ, Urbikain G, López de Lacalle LN, Pereira O, Fernández-Lucio P, Fernández-Valdivielso A. Prediction of cutting forces including tool wear in high-feed turning of Nimonic® C-263 superalloy: A geometric distortion-based model. Meas J Int Meas Confed. 2023;211(December 2022). https://doi.org/10.1016/j.measurement.2023.112580
- [44] Cha KC, Wang N, Liao JY. Stability analysis for the crankshaft grinding machine subjected to a variable-position worktable. Int J Adv Manuf Technol. 2013;67(1-4):501-16. https://doi.org/10.1007/s00170-012-4501-9
- [45] Zaeh MF, Kleinwort R, Fagerer P, Altintas Y. Automatic tuning of active vibration control systems using inertial actuators. CIRP Ann Manuf Technol. 2017;66(1):365-8. https://doi.org/10.1016/j.cirp.2017.04.051
- [46] Azka M, Yamada K, Huda M Al, Tanaka R, Sekiya K. Influence of Tool Posture and Position on Stability in Milling with Parallel Kinematic Machine Tool. Int. J. Precis Eng Manuf [Internet]. 2020;21(12):2359-73. https://doi.org/10.1007/s12541-020-00416-7
- [47] Mehrabadi IM, Nouri M, Madoliat R. Investigating chatter vibration in deep drilling, including process damping and the gyroscopic effect. Int J Mach Tools Manuf. 2009;49(2):939-946. https://doi.org/10.1016/j.ijmachtools.2009.06.009
- [48] Jing W, Hong Z, Gang X, Erbing W, Xiang L. Operational modal analysis for automobile. In: Lecture Notes in Electrical Engineering. 2012. p. 525-32. https://doi.org/10.1007/978-3-642-27311-7_70
- [49] Li X, Luan F, Wu Y. A comparative assessment of six machine learning models for prediction of bending force in hot strip rolling process. Metals (Basel). 2020;10(5). https://doi.org/10.3390/met10050685
- [50] Sadílek M, Dubský J, Sadílková Z, Poruba Z. Cutting forces during turning with variable depth of cut. Perspect Sci. 2016;7:357-63. https://doi.org/10.1016/j.pisc.2015.11.055
- [51] Altintas Y. Manufacturing Automation: Metal Cutting Mechanics, Machine Tool Vibrations, and CNC Design. Cambridge University Press Cambridge, New York. Cambridge University Press Cambridge, New York; 2012. 1-365. https://doi.org/10.1017/CB09780511843723
- [52] Hadji L, Plevris V, Madan R, Ait Atmane H. Multi-Directional Functionally Graded Sandwich Plates: Buckling and Free Vibration Analysis with Refined Plate Models under Various Boundary Conditions. Computation. 2024;12(4). https://doi.org/10.3390/computation12040065
- [53] Tlusty G. Manufacturing Processes and Equipment. New Jersey: Practice-Hall; 2020.